Study of the doubly Cabibbo-suppressed decays $D_s^+ \to K^+K^+\pi^-$ and $D_s^+ \to K^+K^+\pi^-\pi^0$

M. Ablikim,[1] M. N. Achasov,[4,b] P. Adlarson,[75] X. C. Ai,[81] R. Aliberti,[35] A. Amoroso,[74a,74c] M. R. An,[39] Q. An,[71,58] Y. Bai,[57] O. Bakina,[36] I. Balossino,[29a] Y. Ban,[46,g] H.-R. Bao,[63] V. Batozskaya,[1,44] K. Begzsuren,[32] N. Berger,[35] M. Berlowski,[44] M. Bertani,[28a] D. Bettoni,[29a] F. Bianchi,[74a,74c] E. Bianco,[74a,74c] A. Bortone,[74a,74c] I. Boyko,[36] R. A. Briere,[5] A. Brueggemann,[68] H. Cai,[76] X. Cai,[1,58] A. Calcaterra,[28a] G. F. Cao,[1,63] N. Cao,[1,63] S. A. Cetin,[62a] J. F. Chang,[1,58] T. T. Chang,[77] W. L. Chang,[1,63] G. R. Che,[43] G. Chelkov,[36,a] C. Chen,[43] Chao Chen,[55] G. Chen,[1] H. S. Chen,[1,63] M. L. Chen,[1,58,63] S. J. Chen,[42] S. L. Chen,[45] S. M. Chen,[61] T. Chen,[1,63] X. R. Chen,[31,63] X. T. Chen,[1,63] Y. B. Chen,[1,58] Y. Q. Chen,[34] Z. J. Chen,[25,h] S. K. Choi,[10] X. Chu,[43] G. Cibinetto,[29a] S. C. Coen,[3] F. Cossio,[74c] J. J. Cui,[50] H. L. Dai,[1,58] J. P. Dai,[79] A. Dbeyssi,[18] R. E. de Boer,[3] D. Dedovich,[36] Z. Y. Deng,[1] A. Denig,[35] I. Denysenko,[36] M. Destefanis,[74a,74c] F. De Mori,[74a,74c] B. Ding,[66,1] X. X. Ding,[46,g] Y. Ding,[40] Y. Ding,[34] J. Dong,[1,58] L. Y. Dong,[1,63] M. Y. Dong,[1,58,63] X. Dong,[76] M. C. Du,[1] S. X. Du,[81] Z. H. Duan,[42] P. Egorov,[36,a] Y. H. Fan,[45] J. Fang,[1,58] S. S. Fang,[1,63] W. X. Fang,[1] Y. Fang,[1] Y. Q. Fang,[1,58] R. Farinelli,[29a] L. Fava,[74b,74c] F. Feldbauer,[3] G. Felici,[28a] C. Q. Feng,[71,58] J. H. Feng,[59] Y. T. Feng,[71] K. Fischer,[69] M. Fritsch,[3] C. D. Fu,[1] J. L. Fu,[63] Y. W. Fu,[1] H. Gao,[63] Y. N. Gao,[46,g] Yang Gao,[71,58] S. Garbolino,[74c] I. Garzia,[29a,29b] P. T. Ge,[76] Z. W. Ge,[42] C. Geng,[59] E. M. Gersabeck,[67] A. Gilman,[69] K. Goetzen,[13] L. Gong,[40] W. X. Gong,[1,58] W. Gradl,[35] S. Gramigna,[29a,29b] M. Greco,[74a,74c] M. H. Gu,[1,58] Y. T. Gu,[15] C. Y. Guan,[1,63] Z. L. Guan,[22] A. Q. Guo,[31,63] L. B. Guo,[41] M. J. Guo,[50] R. P. Guo,[49] Y. P. Guo,[12,f] A. Guskov,[36,a] J. Gutierrez,[27] T. T. Han,[1] W. Y. Han,[39] X. Q. Hao,[19] F. A. Harris,[65] K. K. He,[55] K. L. He,[1,63] F. H. H. Heinsius,[3] C. H. Heinz,[35] Y. K. Heng,[1,58,63] C. Herold,[60] T. Holtmann,[3] P. C. Hong,[12,f] G. Y. Hou,[1,63] X. T. Hou,[1,63] Y. R. Hou,[63] Z. L. Hou,[1] B. Y. Hu,[59] H. M. Hu,[1,63] J. F. Hu,[56,i] T. Hu,[1,58,63] Y. Hu,[1] G. S. Huang,[71,58] K. X. Huang,[59] L. Q. Huang,[31,63] X. T. Huang,[50] Y. P. Huang,[1] T. Hussain,[73] N. Hüsken,[27,35] N. in der Wiesche,[68] M. Irshad,[71,58] J. Jackson,[27] S. Jaeger,[3] S. Janchiv,[32] J. H. Jeong,[10] Q. Ji,[1] Q. P. Ji,[19] X. B. Ji,[1,63] X. L. Ji,[1,58] Y. Y. Ji,[50] X. Q. Jia,[50] Z. K. Jia,[71,58] H. J. Jiang,[76] P. C. Jiang,[46,g] S. S. Jiang,[39] T. J. Jiang,[16] X. S. Jiang,[1,58,63] Y. Jiang,[63] J. B. Jiao,[50] Z. Jiao,[23] S. Jin,[42] Y. Jin,[66] M. Q. Jing,[1,63] X. M. Jing,[63] T. Johansson,[75] X. K.,[1] S. Kabana,[33] N. Kalantar-Nayestanaki,[64] X. L. Kang,[9] X. S. Kang,[40] M. Kavatsyuk,[64] B. C. Ke,[81] V. Khachatryan,[27] A. Khoukaz,[68] R. Kiuchi,[1] R. Kliemt,[13] O. B. Kolcu,[62a] B. Kopf,[3] M. Kuessner,[3] A. Kupsc,[44,75] W. Kühn,[37] J. J. Lane,[67] P. Larin,[18] A. Lavania,[26] L. Lavezzi,[74a,74c] T. T. Lei,[71,58] Z. H. Lei,[71,58] H. Leithoff,[35] M. Lellmann,[35] T. Lenz,[35] C. Li,[47] C. Li,[43] C. H. Li,[39] Cheng Li,[71,58] D. M. Li,[81] F. Li,[1,58] G. Li,[1] H. Li,[71,58] H. B. Li,[1,63] H. J. Li,[19] H. N. Li,[56,i] Hui Li,[43] J. R. Li,[61] J. S. Li,[59] J. W. Li,[50] Ke Li,[1] L. J. Li,[1,63] L. K. Li,[1] Lei Li,[48] M. H. Li,[43] P. R. Li,[38,k] Q. X. Li,[50] S. X. Li,[12] T. Li,[50] W. D. Li,[1,63] W. G. Li,[1] X. H. Li,[71,58] X. L. Li,[50] Xiaoyu Li,[1,63] Y. G. Li,[46,g] Z. J. Li,[59] Z. X. Li,[15] C. Liang,[42] H. Liang,[71,58] H. Liang,[1,63] Y. F. Liang,[54] Y. T. Liang,[31,63] G. R. Liao,[14] L. Z. Liao,[50] Y. P. Liao,[1,63] J. Libby,[26] A. Limphirat,[60] D. X. Lin,[31,63] T. Lin,[1] B. J. Liu,[1] B. X. Liu,[76] C. Liu,[34] C. X. Liu,[1] F. H. Liu,[53] Fang Liu,[1] Feng Liu,[6] G. M. Liu,[56,i] H. Liu,[38,j,k] H. B. Liu,[15] H. M. Liu,[1,63] Huanhuan Liu,[1] Huihui Liu,[21] J. B. Liu,[71,58] J. Y. Liu,[1,63] K. Liu,[1] K. Y. Liu,[40] Ke Liu,[22] L. Liu,[71,58] L. C. Liu,[43] Lu Liu,[43] M. H. Liu,[12,f] P. L. Liu,[1] Q. Liu,[63] S. B. Liu,[71,58] T. Liu,[12,f] W. K. Liu,[43] W. M. Liu,[71,58] X. Liu,[38,j,k] Y. Liu,[81] Y. Liu,[38,j,k] Y. B. Liu,[43] Z. A. Liu,[1,58,63] Z. Q. Liu,[50] X. C. Lou,[1,58,63] F. X. Lu,[59] H. J. Lu,[23] J. G. Lu,[1,58] X. L. Lu,[1] Y. Lu,[7] Y. P. Lu,[1,58] Z. H. Lu,[1,63] C. L. Luo,[41] M. X. Luo,[80] T. Luo,[12,f] X. L. Luo,[1,58] X. R. Lyu,[63] Y. F. Lyu,[43] F. C. Ma,[40] H. Ma,[79] H. L. Ma,[1] J. L. Ma,[1,63] L. L. Ma,[50] M. M. Ma,[1,63] Q. M. Ma,[1] R. Q. Ma,[1,63] X. Y. Ma,[1,58] Y. Ma,[46,g] Y. M. Ma,[31] F. E. Maas,[18] M. Maggiora,[74a,74c] S. Malde,[69] Q. A. Malik,[73] A. Mangoni,[28b] Y. J. Mao,[46,g] Z. P. Mao,[1] S. Marcello,[74a,74c] Z. X. Meng,[66] J. G. Messchendorp,[13,64] G. Mezzadri,[29a] H. Miao,[1,63] T. J. Min,[42] R. E. Mitchell,[27] X. H. Mo,[1,58,63] B. Moses,[27] N. Yu. Muchnoi,[4,b] J. Muskalla,[35] Y. Nefedov,[36] F. Nerling,[18,d] I. B. Nikolaev,[4,b] Z. Ning,[1,58] S. Nisar,[11,l] Q. L. Niu,[38,j,k] W. D. Niu,[55] Y. Niu,[50] S. L. Olsen,[63] Q. Ouyang,[1,58,63] S. Pacetti,[28b,28c] X. Pan,[55] Y. Pan,[57] A. Pathak,[34] P. Patteri,[28a] Y. P. Pei,[71,58] M. Pelizaeus,[3] H. P. Peng,[71,58] Y. Y. Peng,[38,j,k] K. Peters,[13,d] J. L. Ping,[41] R. G. Ping,[1,63] S. Plura,[35] V. Prasad,[33] F. Z. Qi,[1] H. Qi,[71,58] H. R. Qi,[61] M. Qi,[42] T. Y. Qi,[12,f] S. Qian,[1,58] W. B. Qian,[63] C. F. Qiao,[63] J. J. Qin,[72] L. Q. Qin,[14] X. S. Qin,[50] Z. H. Qin,[1,58] J. F. Qiu,[1] S. Q. Qu,[61] C. F. Redmer,[35] K. J. Ren,[39] A. Rivetti,[74c] M. Rolo,[74c] G. Rong,[1,63] Ch. Rosner,[18] S. N. Ruan,[43] N. Salone,[44] A. Sarantsev,[36,c] Y. Schelhaas,[35] K. Schoenning,[75] M. Scodeggio,[29a,29b] K. Y. Shan,[12,f] W. Shan,[24] X. Y. Shan,[71,58] J. F. Shangguan,[55] L. G. Shao,[1,63] M. Shao,[71,58] C. P. Shen,[12,f] H. F. Shen,[1,63] W. H. Shen,[63] X. Y. Shen,[1,63] B. A. Shi,[63] H. C. Shi,[71,58] J. L. Shi,[12] J. Y. Shi,[1] Q. Q. Shi,[55] R. S. Shi,[1,63] X. Shi,[1,58] J. J. Song,[19] T. Z. Song,[59] W. M. Song,[34,1] Y. J. Song,[12] Y. X. Song,[46,g] S. Sosio,[74a,74c] S. Spataro,[74a,74c] F. Stieler,[35] Y. J. Su,[63] G. B. Sun,[76] G. X. Sun,[1] H. Sun,[63] H. K. Sun,[1] J. F. Sun,[19] K. Sun,[61] L. Sun,[76] S. S. Sun,[1,63] T. Sun,[51,e] W. Y. Sun,[34] Y. Sun,[9] Y. J. Sun,[71,58] Y. Z. Sun,[1] Z. T. Sun,[50] Y. X. Tan,[71,58] C. J. Tang,[54] G. Y. Tang,[1] J. Tang,[59] Y. A. Tang,[76] L. Y. Tao,[72] Q. T. Tao,[25,h] M. Tat,[69] J. X. Teng,[71,58] V. Thoren,[75] W. H. Tian,[52] W. H. Tian,[59] Y. Tian,[31,63] Z. F. Tian,[76] I. Uman,[62b] Y. Wan,[55] S. J. Wang,[50] B. Wang,[1] B. L. Wang,[63] Bo Wang,[71,58]

C. W. Wang,[42] D. Y. Wang,[46,g] F. Wang,[72] H. J. Wang,[38,j,k] J. P. Wang,[50] K. Wang,[1,58] L. L. Wang,[1] M. Wang,[50] Meng Wang,[1,63] N. Y. Wang,[63] S. Wang,[12,f] S. Wang,[38,j,k] T. Wang,[12,f] T. J. Wang,[43] W. Wang,[72] W. Wang,[59] W. P. Wang,[71,58] X. Wang,[46,g] X. F. Wang,[38,j,k] X. J. Wang,[39] X. L. Wang,[12,f] Y. Wang,[61] Y. D. Wang,[45] Y. F. Wang,[1,58,63] Y. L. Wang,[19] Y. N. Wang,[45] Y. Q. Wang,[1] Yaqian Wang,[17,1] Yi Wang,[61] Z. Wang,[1,58] Z. L. Wang,[72] Z. Y. Wang,[1,63] Ziyi Wang,[63] D. Wei,[70] D. H. Wei,[14] F. Weidner,[68] S. P. Wen,[1] C. W. Wenzel,[3] U. Wiedner,[3] G. Wilkinson,[69] M. Wolke,[75] L. Wollenberg,[3] C. Wu,[39] J. F. Wu,[1,8] L. H. Wu,[1] L. J. Wu,[1,63] X. Wu,[12,f] X. H. Wu,[34] Y. Wu,[71] Y. H. Wu,[55] Y. J. Wu,[31] Z. Wu,[1,58] L. Xia,[71,58] X. M. Xian,[39] T. Xiang,[46,g] D. Xiao,[38,j,k] G. Y. Xiao,[42] S. Y. Xiao,[1] Y. L. Xiao,[12,f] Z. J. Xiao,[41] C. Xie,[42] X. H. Xie,[46,g] Y. Xie,[50] Y. G. Xie,[1,58] Y. H. Xie,[6] Z. P. Xie,[71,58] T. Y. Xing,[1,63] C. F. Xu,[1,63] C. J. Xu,[59] G. F. Xu,[1] H. Y. Xu,[66] Q. J. Xu,[16] Q. N. Xu,[30] W. Xu,[1] W. L. Xu,[66] X. P. Xu,[55] Y. C. Xu,[78] Z. P. Xu,[42] Z. S. Xu,[63] F. Yan,[12,f] L. Yan,[12,f] W. B. Yan,[71,58] W. C. Yan,[81] X. Q. Yan,[1] H. J. Yang,[51,e] H. L. Yang,[34] H. X. Yang,[1] Tao Yang,[1] Y. Yang,[12,f] Y. F. Yang,[43] Y. X. Yang,[1,63] Yifan Yang,[1,63] Z. W. Yang,[38,j,k] Z. P. Yao,[50] M. Ye,[1,58] M. H. Ye,[8] J. H. Yin,[1] Z. Y. You,[59] B. X. Yu,[1,58,63] C. X. Yu,[43] G. Yu,[1,63] J. S. Yu,[25,h] T. Yu,[72] X. D. Yu,[46,g] C. Z. Yuan,[1,63] L. Yuan,[2] S. C. Yuan,[1] Y. Yuan,[1,63] Z. Y. Yuan,[59] C. X. Yue,[39] A. A. Zafar,[73] F. R. Zeng,[50] S. H. Zeng,[72] X. Zeng,[12,f] Y. Zeng,[25,h] Y. J. Zeng,[1,63] X. Y. Zhai,[34] Y. C. Zhai,[50] Y. H. Zhan,[59] A. Q. Zhang,[1,63] B. L. Zhang,[1,63] B. X. Zhang,[1] D. H. Zhang,[43] G. Y. Zhang,[19] H. Zhang,[71] H. C. Zhang,[1,58,63] H. H. Zhang,[59] H. H. Zhang,[34] H. Q. Zhang,[1,58,63] H. Y. Zhang,[1,58] J. Zhang,[81] J. Zhang,[59] J. J. Zhang,[52] J. L. Zhang,[20] J. Q. Zhang,[41] J. W. Zhang,[1,58,63] J. X. Zhang,[38,j,k] J. Y. Zhang,[1] J. Z. Zhang,[1,63] Jianyu Zhang,[63] L. M. Zhang,[61] L. Q. Zhang,[59] Lei Zhang,[42] P. Zhang,[1,63] Q. Y. Zhang,[39,81] Shuihan Zhang,[1,63] Shulei Zhang,[25,h] X. D. Zhang,[45] X. M. Zhang,[1] X. Y. Zhang,[50] Y. Zhang,[69] Y. Zhang,[72] Y. T. Zhang,[81] Y. H. Zhang,[1,58] Yan Zhang,[71,58] Yao Zhang,[1] Z. D. Zhang,[1] Z. H. Zhang,[1] Z. L. Zhang,[34] Z. Y. Zhang,[43] Z. Y. Zhang,[76] G. Zhao,[1] J. Y. Zhao,[1,63] J. Z. Zhao,[1,58] Lei Zhao,[71,58] Ling Zhao,[1] M. G. Zhao,[43] R. P. Zhao,[63] S. J. Zhao,[81] Y. B. Zhao,[1,58] Y. X. Zhao,[31,63] Z. G. Zhao,[71,58] A. Zhemchugov,[36,a] B. Zheng,[72] J. P. Zheng,[1,58] W. J. Zheng,[1,63] Y. H. Zheng,[63] B. Zhong,[41] X. Zhong,[59] H. Zhou,[50] L. P. Zhou,[1,63] X. Zhou,[76] X. K. Zhou,[6] X. R. Zhou,[71,58] X. Y. Zhou,[39] Y. Z. Zhou,[12,f] J. Zhu,[43] K. Zhu,[1] K. J. Zhu,[1,58,63] L. Zhu,[34] L. X. Zhu,[63] S. H. Zhu,[70] S. Q. Zhu,[42] T. J. Zhu,[12,f] W. J. Zhu,[12,f] Y. C. Zhu,[71,58] Z. A. Zhu,[1,63] J. H. Zou,[1] and J. Zu[71,58]

(BESIII Collaboration)

[1]*Institute of High Energy Physics, Beijing 100049, People's Republic of China*
[2]*Beihang University, Beijing 100191, People's Republic of China*
[3]*Bochum Ruhr-University, D-44780 Bochum, Germany*
[4]*Budker Institute of Nuclear Physics SB RAS (BINP), Novosibirsk 630090, Russia*
[5]*Carnegie Mellon University, Pittsburgh, Pennsylvania 15213, USA*
[6]*Central China Normal University, Wuhan 430079, People's Republic of China*
[7]*Central South University, Changsha 410083, People's Republic of China*
[8]*China Center of Advanced Science and Technology, Beijing 100190, People's Republic of China*
[9]*China University of Geosciences, Wuhan 430074, People's Republic of China*
[10]*Chung-Ang University, Seoul, 06974, Republic of Korea*
[11]*COMSATS University Islamabad, Lahore Campus, Defence Road, Off Raiwind Road, 54000 Lahore, Pakistan*
[12]*Fudan University, Shanghai 200433, People's Republic of China*
[13]*GSI Helmholtzcentre for Heavy Ion Research GmbH, D-64291 Darmstadt, Germany*
[14]*Guangxi Normal University, Guilin 541004, People's Republic of China*
[15]*Guangxi University, Nanning 530004, People's Republic of China*
[16]*Hangzhou Normal University, Hangzhou 310036, People's Republic of China*
[17]*Hebei University, Baoding 071002, People's Republic of China*
[18]*Helmholtz Institute Mainz, Staudinger Weg 18, D-55099 Mainz, Germany*
[19]*Henan Normal University, Xinxiang 453007, People's Republic of China*
[20]*Henan University, Kaifeng 475004, People's Republic of China*
[21]*Henan University of Science and Technology, Luoyang 471003, People's Republic of China*
[22]*Henan University of Technology, Zhengzhou 450001, People's Republic of China*
[23]*Huangshan College, Huangshan 245000, People's Republic of China*
[24]*Hunan Normal University, Changsha 410081, People's Republic of China*
[25]*Hunan University, Changsha 410082, People's Republic of China*
[26]*Indian Institute of Technology Madras, Chennai 600036, India*
[27]*Indiana University, Bloomington, Indiana 47405, USA*
[28a]*INFN Laboratori Nazionali di Frascati, I-00044, Frascati, Italy*

[28b]INFN Sezione di Perugia, I-06100, Perugia, Italy
[28c]University of Perugia, I-06100, Perugia, Italy
[29a]INFN Sezione di Ferrara, I-44122, Ferrara, Italy
[29b]University of Ferrara, I-44122, Ferrara, Italy
[30]Inner Mongolia University, Hohhot 010021, People's Republic of China
[31]Institute of Modern Physics, Lanzhou 730000, People's Republic of China
[32]Institute of Physics and Technology, Peace Avenue 54B, Ulaanbaatar 13330, Mongolia
[33]Instituto de Alta Investigación, Universidad de Tarapacá, Casilla 7D, Arica 1000000, Chile
[34]Jilin University, Changchun 130012, People's Republic of China
[35]Johannes Gutenberg University of Mainz, Johann-Joachim-Becher-Weg 45, D-55099 Mainz, Germany
[36]Joint Institute for Nuclear Research, 141980 Dubna, Moscow region, Russia
[37]Justus-Liebig-Universitaet Giessen, II. Physikalisches Institut, Heinrich-Buff-Ring 16, D-35392 Giessen, Germany
[38]Lanzhou University, Lanzhou 730000, People's Republic of China
[39]Liaoning Normal University, Dalian 116029, People's Republic of China
[40]Liaoning University, Shenyang 110036, People's Republic of China
[41]Nanjing Normal University, Nanjing 210023, People's Republic of China
[42]Nanjing University, Nanjing 210093, People's Republic of China
[43]Nankai University, Tianjin 300071, People's Republic of China
[44]National Centre for Nuclear Research, Warsaw 02-093, Poland
[45]North China Electric Power University, Beijing 102206, People's Republic of China
[46]Peking University, Beijing 100871, People's Republic of China
[47]Qufu Normal University, Qufu 273165, People's Republic of China
[48]Renmin University of China, Beijing 100872, People's Republic of China
[49]Shandong Normal University, Jinan 250014, People's Republic of China
[50]Shandong University, Jinan 250100, People's Republic of China
[51]Shanghai Jiao Tong University, Shanghai 200240, People's Republic of China
[52]Shanxi Normal University, Linfen 041004, People's Republic of China
[53]Shanxi University, Taiyuan 030006, People's Republic of China
[54]Sichuan University, Chengdu 610064, People's Republic of China
[55]Soochow University, Suzhou 215006, People's Republic of China
[56]South China Normal University, Guangzhou 510006, People's Republic of China
[57]Southeast University, Nanjing 211100, People's Republic of China
[58]State Key Laboratory of Particle Detection and Electronics, Beijing 100049, Hefei 230026, People's Republic of China
[59]Sun Yat-Sen University, Guangzhou 510275, People's Republic of China
[60]Suranaree University of Technology, University Avenue 111, Nakhon Ratchasima 30000, Thailand
[61]Tsinghua University, Beijing 100084, People's Republic of China
[62a]Turkish Accelerator Center Particle Factory Group, Istinye University, 34010, Istanbul, Turkey
[62b]Near East University, Nicosia, North Cyprus, 99138, Mersin 10, Turkey
[63]University of Chinese Academy of Sciences, Beijing 100049, People's Republic of China
[64]University of Groningen, NL-9747 AA Groningen, The Netherlands
[65]University of Hawaii, Honolulu, Hawaii 96822, USA
[66]University of Jinan, Jinan 250022, People's Republic of China
[67]University of Manchester, Oxford Road, Manchester M13 9PL, United Kingdom
[68]University of Muenster, Wilhelm-Klemm-Strasse 9, 48149 Muenster, Germany
[69]University of Oxford, Keble Road, Oxford OX13RH, United Kingdom
[70]University of Science and Technology Liaoning, Anshan 114051, People's Republic of China
[71]University of Science and Technology of China, Hefei 230026, People's Republic of China
[72]University of South China, Hengyang 421001, People's Republic of China
[73]University of the Punjab, Lahore-54590, Pakistan
[74a]University of Turin and INFN, University of Turin, I-10125, Turin, Italy
[74b]University of Eastern Piedmont, I-15121, Alessandria, Italy
[74c]INFN, I-10125, Turin, Italy
[75]Uppsala University, Box 516, SE-75120 Uppsala, Sweden
[76]Wuhan University, Wuhan 430072, People's Republic of China
[77]Xinyang Normal University, Xinyang 464000, People's Republic of China
[78]Yantai University, Yantai 264005, People's Republic of China

[79]Yunnan University, Kunming 650500, People's Republic of China
[80]Zhejiang University, Hangzhou 310027, People's Republic of China
[81]Zhengzhou University, Zhengzhou 450001, People's Republic of China

(Received 24 October 2023; accepted 30 January 2024; published 27 February 2024)

Based on 7.33 fb^{-1} of e^+e^- collision data collected at center-of-mass energies between 4.128 and 4.226 GeV with the BESIII detector, the experimental studies of the doubly Cabibbo-suppressed decays $D_s^+ \to K^+K^+\pi^-$ and $D_s^+ \to K^+K^+\pi^-\pi^0$ are reported. We determine the absolute branching fraction of $D_s^+ \to K^+K^+\pi^-$ to be $(1.24^{+0.28}_{-0.26}(\mathrm{stat}) \pm 0.06(\mathrm{syst})) \times 10^{-4}$. No significant signal of $D_s^+ \to K^+K^+\pi^-\pi^0$ is observed and the upper limit on its decay branching fraction at 90% confidence level is set to be 1.7×10^{-4}.

DOI: 10.1103/PhysRevD.109.032011

I. INTRODUCTION

Doubly Cabibbo-suppressed (DCS) decays of charmed mesons offer a unique platform to understand the dynamics of charmed mesons. It is naively expected that the ratio of the branching fraction between a given DCS D decay and its Cabibbo-favored (CF) counterpart is about $(0.5-2.0) \times \tan^4\theta_C$, where θ_C is the Cabibbo mixing angle [1,2]. In 2020 and 2021, BESIII reported [3,4] the observation of the DCS decay $D^+ \to K^+\pi^+\pi^-\pi^0$ (charge conjugate decays are always implied throughout this paper). The average branching fraction of $D^+ \to K^+\pi^+\pi^-\pi^0$, weighted from the two measurements in [3,4], is $[1.13 \pm 0.08(\mathrm{stat}) \pm 0.03(\mathrm{syst})] \times 10^{-3}$. This gives a DCS/CF branching fraction ratio of $(6.3 \pm 0.5)\tan^4\theta_C$. Further measurements of the DCS decays of charmed mesons may shed light on the decay dynamics. Specifically, two-body DCS D decay branching fractions are important inputs to help understand quark SU(3)-flavor symmetry and its breaking effects in the charm sector [5–11].

In the D_s^+ sector, only the DCS decay $D_s^+ \to K^+K^+\pi^-$ was previously reported [12]. Its decay branching fraction was measured relative to the CF decay of $D_s^+ \to K^+K^-\pi^+$ by LHCb, *BABAR*, Belle, and FOCUS [13–16]. In this article, we present the first measurement of absolute branching fraction of $D_s^+ \to K^+K^+\pi^-$ and search for $D_s^+ \to K^+K^+\pi^-\pi^0$ for the first time. This analysis uses the e^+e^- collision data samples collected at center-of-mass energies ($E_{\mathrm{c.m.}}$) between 4.128 and 4.226 GeV with the BESIII detector, corresponding to an integrated luminosity of 7.33 fb^{-1} [17].

II. BESIII DETECTOR AND MONTE CARLO SIMULATION

The BESIII detector [18] is a magnetic spectrometer located at the Beijing Electron Positron Collider (BEPCII) [19]. The cylindrical core of the BESIII detector consists of a helium-based multilayer drift chamber (MDC), a plastic scintillator time-of-flight system (TOF), and a CsI(Tl) electromagnetic calorimeter (EMC), which are all enclosed in a superconducting solenoidal magnet providing a 1.0 T magnetic field. The solenoid is supported by an octagonal flux-return yoke with resistive plate counter muon identifier modules interleaved with steel. The acceptance of charged particles and photons is 93% over 4π solid angle. The charged particle momentum resolution at 1 GeV$/c$ is 0.5%, and the specific ionization energy loss dE/dx resolution is 6% for the electrons from Bhabha scattering. The EMC measures photon energies with a resolution of 2.5% (5%) at

[a]Also at the Moscow Institute of Physics and Technology, Moscow 141700, Russia.
[b]Also at the Novosibirsk State University, Novosibirsk, 630090, Russia.
[c]Also at the NRC "Kurchatov Institute," PNPI, 188300, Gatchina, Russia.
[d]Also at Goethe University Frankfurt, 60323 Frankfurt am Main, Germany.
[e]Also at Key Laboratory for Particle Physics, Astrophysics and Cosmology, Ministry of Education; Shanghai Key Laboratory for Particle Physics and Cosmology; Institute of Nuclear and Particle Physics, Shanghai 200240, People's Republic of China.
[f]Also at Key Laboratory of Nuclear Physics and Ion-beam Application (MOE) and Institute of Modern Physics, Fudan University, Shanghai 200443, People's Republic of China.
[g]Also at State Key Laboratory of Nuclear Physics and Technology, Peking University, Beijing 100871, People's Republic of China.
[h]Also at School of Physics and Electronics, Hunan University, Changsha 410082, China.
[i]Also at Guangdong Provincial Key Laboratory of Nuclear Science, Institute of Quantum Matter, South China Normal University, Guangzhou 510006, China.
[j]Also at MOE Frontiers Science Center for Rare Isotopes, Lanzhou University, Lanzhou 730000, People's Republic of China.
[k]Also at Lanzhou Center for Theoretical Physics, Lanzhou University, Lanzhou 730000, People's Republic of China.
[l]Also at the Department of Mathematical Sciences, IBA, Karachi 75270, Pakistan.

1 GeV in the barrel (end cap) region. The time resolution of the TOF barrel section is 68 ps, while that of the end cap portion is 110 ps. The end cap TOF system was upgraded in 2015 using multigap resistive plate chamber technology, providing a time resolution of 60 ps [20], which benefits 83% of the data used in this analysis [21,22].

Simulated samples produced with the Geant4-based [23] Monte Carlo (MC) package which includes the geometric description of the BESIII detector and the detector response, are used to determine the detection efficiency and to estimate the backgrounds. The simulation includes the beam energy spread and initial state radiation (ISR) of the e^+e^- annihilations modeled with the generator KKMC [24]. The inclusive MC samples consist of the production of $D_s^{(*)}\overline{D_{(s)}^{(*)}}$ pairs (with consideration of quantum coherence for all $D^0\bar{D}^0$ pair decays), the non-$D\bar{D}$ decays of the $\psi(3770)$, the ISR production of the J/ψ and $\psi(3686)$ states, and the continuum processes. The known decay modes are modeled with EvtGen [25] using the branching fractions taken from the Particle Data Group (PDG) [12], and the remaining unknown decays of the charmonium states with LUNDCHARM [26]. Final state radiation from charged final state particles is incorporated with the PHOTOS package [27]. The signal MC sample of $D_s^+ \to K^+K^+\pi^-$ is generated using the known fraction of the intermediate channel $D_s^+ \to K^+K^{*0}$ [12], while the unknown subchannels are generated according to the phase space. The signal MC sample of $D_s^+ \to K^+K^+\pi^-\pi^0$ is also generated uniformly over the phase space.

III. MEASUREMENT METHOD

In the e^+e^- collision data taken at $E_{\mathrm{c.m.}}$ between 4.128 and 4.226 GeV, the $D_s^\pm$ mesons are produced mainly via the $e^+e^- \to D_s^{*\pm}D_s^\mp \to \gamma(\pi^0)D_s^+D_s^-$ process. This analysis is performed by using the double-tag (DT) method pioneered by the MARKIII collaboration [28]. A D_s^- meson which is fully reconstructed via one of the eleven hadronic decay modes is referred to as a single-tag (ST) D_s^- meson. The event, in which the $\gamma(\pi^0)$ emitted from D_s^{*+} and the signal decay can be successfully reconstructed in the presence of ST D_s^- meson, is called as a DT event. The branching fraction of the signal decay is determined as

$$\mathcal{B}_{\mathrm{sig}} = \frac{N_{\mathrm{DT}}}{N_{\mathrm{ST}} \cdot \epsilon_{\mathrm{sig}}}, \tag{1}$$

where N_{DT} and N_{ST} are the yields of the DT events and ST D_s^- mesons in data, respectively; ϵ_{sig} is the efficiency of detecting the signal decay in the presence of the ST D_s^- mesons, averaged over the $D_s^* \to D_s\gamma$ and $D_s^* \to D_s\pi^0$ transitions weighted by their branching fractions.

IV. ST CANDIDATES

To reconstruct ST D_s^- candidates, we use eleven hadronic decay modes of $D_s^- \to K^+K^-\pi^-$, $K^+K^-\pi^-\pi^0$, $\pi^-\pi^+\pi^-$, $K_S^0K^-$, $K_S^0K^+\pi^-\pi^-$, $\eta_{\gamma\gamma}\pi^-$, $\eta_{\pi^+\pi^-\pi^0}\pi^-$, $\eta'_{\pi^+\pi^-\eta}\pi^-$, $\eta'_{\gamma\rho^0}\pi^-$, $\eta_{\gamma\gamma}\rho^-$, and $\eta_{\pi^+\pi^-\pi^0}\rho^-$. Throughout this article, ρ denotes $\rho(770)$ and the subscripts of $\eta^{(\prime)}$ denote individual decay modes adopted for $\eta^{(\prime)}$ reconstruction.

The $K^\pm$, $\pi^\pm$, K_S^0, γ, π^0, and η candidates are selected with the same criteria as in Refs. [29–31]. All charged tracks, except for those from K_S^0, are required to originate from a region defined as $|V_{xy}| < 1$ and $|V_z| < 10$ cm, where $|V_z|$ and $|V_{xy}|$ are the distances of the closest approach relative to the interaction point along the MDC axis and in the transverse plane, respectively. The track polar angle θ with respect to the MDC axis must satisfy $|\cos\theta| < 0.93$. Charged particles are identified by using the combined dE/dx and TOF information. A particle is assigned to be a pion (kaon) candidate if the confidence level for the corresponding hypothesis is greater than for the kaon (pion) hypothesis.

Candidates for K_S^0 are selected via the decay $K_S^0 \to \pi^+\pi^-$. The two charged pions are required to satisfy $|V_z| < 20$ cm and $|\cos\theta| < 0.93$. They are assumed to be $\pi^+\pi^-$ without particle identification (PID) requirements. The two pions are required to have a common vertex point via a secondary vertex fit; the fit χ^2 must be less than 200 and their invariant mass is required to be within $(0.487, 0.511)$ GeV$/c^2$. The decay length of any K_S^0 candidate, measured from the interaction point, is required to be greater than twice the vertex resolution.

Photon candidates are reconstructed by using shower information measured by the EMC. To suppress backgrounds from electronic noise or bremsstrahlung, candidate showers are required to start within [0, 700] ns from the event start time and the energy of each shower in the barrel (end cap) region of the EMC [18] is required to be greater than 25 (50) MeV. To suppress backgrounds associated with charged tracks, the angle subtended by the EMC shower and the closest charged track extrapolation to the EMC must be greater than 10 degrees as measured from the interaction point.

Candidates for π^0 and $\eta_{\gamma\gamma}$ are formed from $\gamma\gamma$ pairs with invariant masses in the intervals (0.115, 0.150) and $(0.500, 0.570)$ GeV$/c^2$, respectively. To improve momentum resolution, each $\gamma\gamma$ pair is subject to a one-constraint (1C) kinematic fit that constrains their invariant mass to the π^0 or η nominal mass [12]. To form candidates for $\rho^{+(0)}$, $\eta_{\pi^0\pi^+\pi^-}$, $\eta'_{\eta\pi^+\pi^-}$, and $\eta'_{\gamma\rho^0}$, the invariant masses of the $\pi^+\pi^{0(-)}$, $\pi^0\pi^+\pi^-$, $\eta\pi^+\pi^-$, and $\gamma\rho^0$ combinations are required to be within the mass intervals of (0.570, 0.970), (0.530, 0.570), (0.946, 0.970), and (0.940, 0.976) GeV$/c^2$, respectively. In addition, the energy of the γ from an $\eta'_{\gamma\rho^0}$ decay is required to be greater than 0.1 GeV.

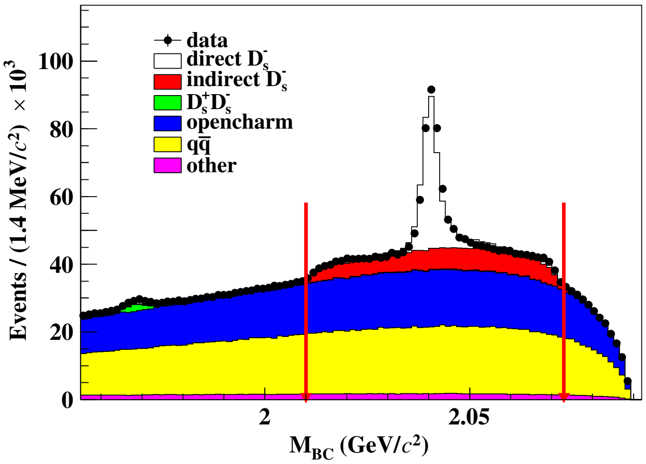

FIG. 1. The $M_{\rm BC}$ distributions of the ST candidates in data and inclusive MC sample at 4.178 GeV. The candidates between the two red arrows are accepted.

The transition pions from D^{*+} decays are suppressed by requiring the momentum of any pion which is not from a K_S^0, η, or η' decay to be greater than 0.1 GeV/c. In order to reject peaking background from the $D_s^- \to K_S^0\pi^-$ final state in the selection of the $D_s^- \to \pi^+\pi^-\pi^-$ tag mode, the invariant mass of each $\pi^+\pi^-$ combination is required to be outside the mass window of $(0.468, 0.528)$ GeV/c^2.

The backgrounds from non-$D_s^\pm D_s^{*\mp}$ processes are suppressed by using the beam-constrained mass of the ST D_s^- candidate, defined as

$$M_{\rm BC} \equiv \sqrt{E_{\rm beam}^2 - |\vec{p}_{\rm tag}|^2}, \tag{2}$$

where $E_{\rm beam}$ is the beam energy and $\vec{p}_{\rm tag}$ is the momentum of the ST D_s^- candidate in the e^+e^- rest frame. Figure 1 shows the $M_{\rm BC}$ distributions of the ST candidates in data and inclusive MC sample at 4.178 GeV. For the direct D_s^- mesons which are produced by the e^+e^- collision, $M_{\rm BC}$ peaks, as shown by the open histogram. For the indirect D_s^- mesons which are produced from D_s^{*-} decays, the $M_{\rm BC}$ distribution is broader, as shown by the red histogram. The $M_{\rm BC}$ value is required to be within the intervals listed in Table I. This requirement retains about 99% of the D_s^- and D_s^+ mesons from $e^+e^- \to D_s^{*\mp}D_s^\pm$.

TABLE I. Requirements of $M_{\rm BC}$ for each energy point.

$E_{\rm c.m.}$ (GeV)	$M_{\rm BC}$ (GeV/c^2)
4.128	[2.010, 2.061]
4.157	[2.010, 2.070]
4.178	[2.010, 2.073]
4.189	[2.010, 2.076]
4.199	[2.010, 2.079]
4.209	[2.010, 2.082]
4.219	[2.010, 2.085]
4.226	[2.010, 2.088]

If there are multiple candidates present per tag mode per charge, only the one with the D_s^- recoil mass

$$M_{\rm rec} \equiv \sqrt{\left(E_{\rm c.m.} - \sqrt{|\vec{p}_{\rm tag}|^2 + m_{D_s^-}^2}\right)^2 - |\vec{p}_{\rm tag}|^2} \tag{3}$$

closest to the D_s^{*+} nominal mass [12] is kept for further analysis. The average correct tag efficiency of the best candidate selection for individual tag modes is about 94%. The distributions of the invariant masses ($M_{\rm tag}$) of the accepted ST candidates for various tag modes are shown in Fig. 2. The yields of ST D_s^- mesons reconstructed in various tag modes are derived from fits to their individual $M_{\rm tag}$ distributions. In the fits, the signal is described by the simulated shape convolved with a Gaussian function to take into account the resolution difference between data and simulation. In the fit to the $D_s^- \to K_S^0K^-$ tag mode, the shape of the peaking background of $D^- \to K_S^0\pi^-$ is modeled by the simulated shape convolved with the same Gaussian resolution function as used for the signal. The combinatorial background is described by first, second or third-order Chebychev polynomial functions. The order of the polynomial has been validated by analyzing the inclusive MC sample. Figure 2 shows the fit results of different tag modes for the combined data sample from all energy points. In each subfigure, the black arrows show the chosen $M_{\rm tag}$ signal regions. The candidates located in these signal regions are kept for further analysis.

Based on simulation, the $e^+e^- \to (\gamma_{\rm ISR})D_s^+D_s^-$ process is found to contribute about (0.7–1.1)% in the fitted yields of ST D_s^- mesons for various tag modes and has been subtracted away from the fitted yields in this analysis. Production of $D_s^{*+}D_s^{*-}$ pairs occurs only at the highest c.m. energy; candidates are suppressed by the $M_{\rm BC}$ requirement and are negligible. The second and third columns of Table II summarize the yields of ST D_s^- mesons ($N_{\rm ST}$) for various tag modes obtained from the combined data sample and the corresponding detection efficiencies ($\epsilon_{\rm ST}$), respectively.

V. DT CANDIDATES

The transition photon (or π^0) and the signal D_s^+ decay candidate are reconstructed from the particles recoiling against the selected D_s^- tag. We define the energy difference $\Delta E \equiv E_{\rm tag} + E^{\rm rec}_{\gamma(\pi^0)+D_s^-} + E_{\gamma(\pi^0)} - E_{\rm c.m.}$, where $E^{\rm rec}_{\gamma(\pi^0)+D_s^-} \equiv \sqrt{|-\vec{p}_{\gamma(\pi^0)} - \vec{p}_{\rm tag}|^2 + M^2_{D_s^+}}$, E_i and $\vec{p}_i$ [$i = \gamma(\pi^0)$ or tag] are the energy and momentum of $\gamma(\pi^0)$ or D_s^- tag, respectively. A loop is performed over all γ and π^0 candidates which were not used in the ST reconstruction, under the two assumptions of $D_s^* \to \pi^0 D_s$ and

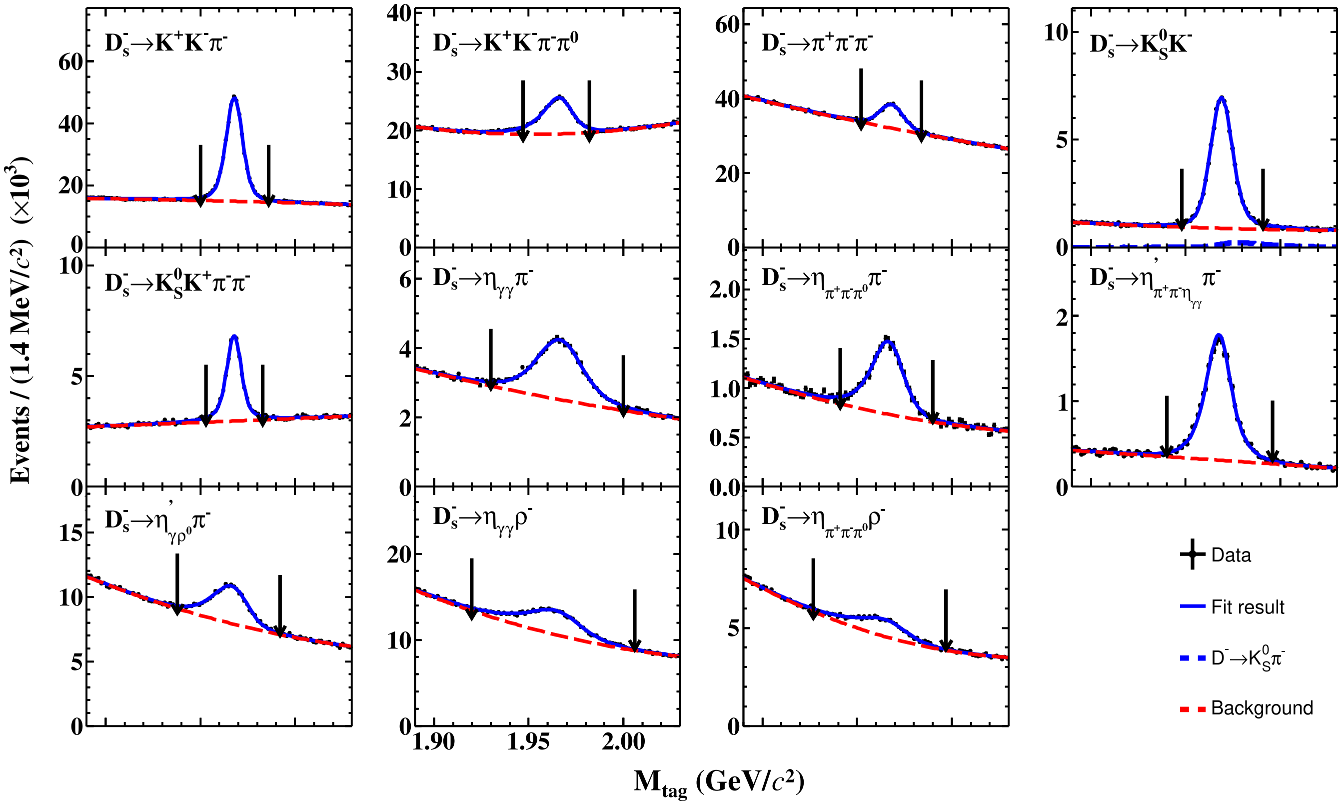

FIG. 2. Fits to the $M_{\rm tag}$ distributions of the selected ST candidates for various tag modes. The points with error bars are the data combined from all energy points. The blue solid curves represent the best fit results, and the red dashed curves stand for the fitted backgrounds. For the tag mode of $D_s^- \to K_S^0K^-$, the blue dashed curve is the peaking background from $D^- \to K_S^0\pi^-$. The pair of arrows denote the $M_{\rm tag}$ signal regions.

$D_s^{*+} \to \gamma D_s^+$. If more than one combination satisfies the selection criteria, the one with the minimum $|\Delta E|$ is chosen.

The selection criteria of π^-, K^+, and π^0 for $D_s^+ \to K^+K^+\pi^-$ and $D_s^+ \to K^+K^+\pi^-\pi^0$ reconstruction are the same as those used to choose the ST candidates. We require that there are exactly three good charged tracks which are not used to form the ST candidate; one track is identified as a π^- and the others are required to be identified as K^+s. For $D_s^+ \to K^+K^+\pi^-\pi^0$, if there are multiple π^0s on the signal side, only the π^0 with the smallest χ^2 of the 1C (mass-constrained) kinematic fit is selected.

Figure 3 shows the distributions of the invariant masses, $M_{\rm sig}$, of the accepted signal candidates. The DT efficiencies and the signal efficiencies of detecting $D_s^+ \to K^+K^+\pi^-$ and $D_s^+ \to K^+K^+\pi^-\pi^0$ for different tag modes, weighted over different energy points, are summarized in Table II. The average signal efficiencies of $D_s^+ \to K^+K^+\pi^-$ and $D_s^+ \to K^+K^+\pi^-\pi^0$, weighted over different tag modes, are $(35.57 \pm 0.18)\%$ and $(10.32 \pm 0.10)\%$, respectively, where the uncertainties are due to the limited MC statistics.

The signal yields are extracted from unbinned maximum likelihood fits to the $M_{\rm sig}$ spectra in Fig. 3. In the fit, the signal is modeled by the MC-simulated signal shape smeared with an additional Gaussian resolution function (with float parameters for $D_s^+ \to K^+K^+\pi^-$ and fixed parameters from a fit to the corresponding CF decays for $D_s^+ \to K^+K^+\pi^-\pi^0$). The background is described by the simulated shape from the inclusive MC sample, and the yields of the signal and background are floating. The statistical significance of $D_s^+ \to K^+K^+\pi^-$ is estimated to be 6.2σ, by $\sqrt{-2\ln(\mathcal{L}_0/\mathcal{L}_{\rm max})}$, where $\mathcal{L}_{\rm max}$ and $\mathcal{L}_0$ are the maximal likelihoods of the fits with and without the signal contribution, respectively. The signal yield of $D_s^+ \to K^+K^+\pi^-$ is obtained to be $33.3^{+7.6}_{-6.9}$.

For $D_s^+ \to K^+K^+\pi^-\pi^0$, no significant signal is observed, and an upper limit on the decay branching fraction is set.

VI. SYSTEMATIC UNCERTAINTIES

Table III summarizes the sources of systematic uncertainty in the branching fraction measurements; details are given below.

The systematic uncertainties on the fitted yields of the ST D_s^- mesons are estimated by using alternative signal and background shapes. First, alternative signal shapes are obtained by changing from those derived from the inclusive

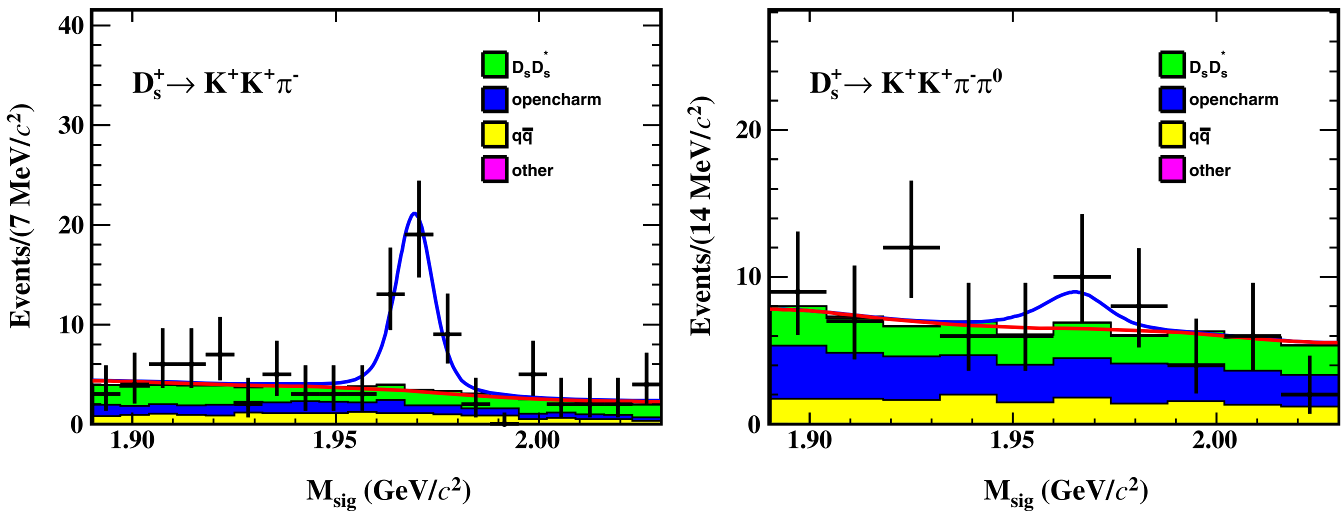

FIG. 3. Fits to the $M_{\rm sig}$ distributions of the accepted DT candidates. The points with error bars are the combined data from all energy points. The blue solid curves are the fit results, the red solid curves are the combinatorial backgrounds, and the histograms filled in colors are from different background sources, derived from the inclusive MC sample and normalized to the fitted background yields in data.

TABLE II. The fitted yields of ST D_s^- mesons from the combined data sample, $N_{\rm ST}$ (in units of $\times 10^3$), the efficiencies of detecting ST D_s^- mesons, DT events, and signal events ($\epsilon_{\rm ST}$, $\epsilon_{\rm DT}$, $\epsilon_{\rm sig} = \epsilon_{\rm DT}/\epsilon_{\rm ST}$, all %) for various tag modes. For all numbers, the uncertainties are statistical only. The listed efficiencies do not include the branching fractions of any daughter particle decays. For each signal channel, the efficiencies have been weighted over different energy points and different ST decay modes.

Tag mode	$M_{\rm tag}$ (GeV/c^2)	$N_{\rm ST}$	$\epsilon_{\rm ST}$	$\epsilon_{{\rm DT},K^+K^+\pi^-}$	$\epsilon_{{\rm sig},K^+K^+\pi^-}$	$\epsilon_{{\rm DT},K^+K^+\pi^-\pi^0}$	$\epsilon_{{\rm sig},K^+K^+\pi^-\pi^0}$
$K^+K^-\pi^-$	(1.950, 1.986)	280.7 ± 0.9	40.87 ± 0.01	13.99 ± 0.06	34.23 ± 0.14	4.24 ± 0.03	10.38 ± 0.09
$K^+K^-\pi^-\pi^0$	(1.947, 1.982)	86.3 ± 1.3	11.83 ± 0.01	4.53 ± 0.09	38.30 ± 0.80	1.08 ± 0.05	9.16 ± 0.44
$\pi^-\pi^+\pi^-$	(1.952, 1.984)	72.7 ± 1.4	51.86 ± 0.03	17.68 ± 0.06	34.09 ± 0.12	5.54 ± 0.04	10.69 ± 0.07
$K_S^0K^-$	(1.948, 1.991)	62.2 ± 0.4	47.37 ± 0.03	16.07 ± 0.07	33.93 ± 0.15	5.07 ± 0.04	10.70 ± 0.09
$K_S^0K^+\pi^-\pi^-$	(1.953, 1.983)	29.6 ± 0.3	20.98 ± 0.03	6.99 ± 0.14	33.31 ± 0.68	1.85 ± 0.08	8.82 ± 0.38
$\eta_{\gamma\gamma}\pi^-$	(1.930, 2.000)	39.6 ± 0.8	48.31 ± 0.04	16.79 ± 0.06	34.76 ± 0.12	5.19 ± 0.03	10.74 ± 0.07
$\eta_{\pi^+\pi^-\pi^0}\pi^-$	(1.941, 1.990)	11.7 ± 0.3	23.31 ± 0.05	8.21 ± 0.06	35.24 ± 0.26	2.35 ± 0.03	10.07 ± 0.15
$\eta'_{\pi^+\pi^-\eta}\pi^-$	(1.940, 1.996)	19.7 ± 0.2	25.17 ± 0.04	8.32 ± 0.06	33.06 ± 0.23	2.46 ± 0.03	9.78 ± 0.13
$\eta'_{\gamma\rho^0}\pi^-$	(1.938, 1.992)	50.4 ± 1.0	32.46 ± 0.03	11.53 ± 0.06	35.51 ± 0.18	3.42 ± 0.03	10.52 ± 0.11
$\eta_{\gamma\gamma}\rho^-$	(1.920, 2.006)	80.1 ± 2.3	19.92 ± 0.01	8.31 ± 0.07	41.72 ± 0.30	2.27 ± 0.04	11.40 ± 0.18
$\eta_{\pi^+\pi^-\pi^0}\rho^-$	(1.927, 1.997)	22.2 ± 1.4	9.15 ± 0.01	3.90 ± 0.07	42.64 ± 0.65	0.98 ± 0.03	10.73 ± 0.38
Weighted average					35.57 ± 0.18		10.32 ± 0.10

MC sample to those from the signal MC samples. Second, an alternative background shape is obtained by varying the order of the nominal Chebychev function by ± 1. For a given ST mode, the differences in the ratio of the yields of ST D_s^- mesons over the corresponding efficiency for all variations, and the background fluctuation of the fitted yield of ST D_s^- are reweighted by the yields of ST D_s^- mesons in various data samples and are added in quadrature. An additional component to this uncertainty is statistical in nature, and accounts for the contribution of background fluctuations to the fitted yields of ST D_s^- mesons. The total uncertainty associated with the ST yield $N_{\rm ST}^{\rm tot}$ is estimated to be 0.5%.

TABLE III. Systematic uncertainties on the branching fraction measurements. Uncertainties in the square brackets are additive uncertainties on the number of events; all other uncertainties are in %.

Source	$K^+K^+\pi^-$	$K^+K^+\pi^-\pi^0$
$N_{\rm ST}$	0.5	0.5
Tracking	3.0	3.0
PID	3.0	3.0
γ, π^0 reconstruction	1.0	3.0
$M_{\rm sig}$ fit	$\cdots$	[0.2]
Quoted branching fractions	0.3	0.3
MC model	0.7	5.3
MC statistics	0.5	1.0
Total	4.5	7.5 [0.2]

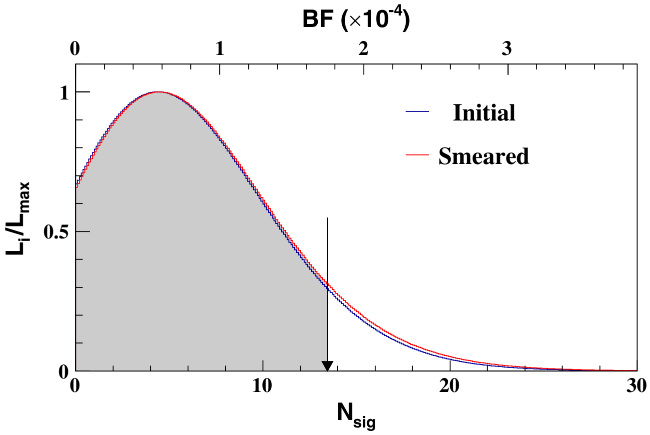

FIG. 4. Distributions of normalized likelihoods versus the branching fraction of $D_s^+ \to K^+K^+\pi^-\pi^0$. The results incorporating the systematic uncertainties are shown as the blue curve. The black arrow shows the $N_{\rm sig}$ result corresponding to 90% confidence level.

The systematic uncertainties from the tracking and PID of $K^\pm$ and $\pi^\pm$ are estimated by using the control sample of $e^+e^- \to K^+K^-\pi^+\pi^-(\pi^0)$ [32]. The systematic uncertainties in the tracking and PID efficiencies are both assigned as 1.0% per $K^\pm$ or $\pi^\pm$. The systematic uncertainties in the photon selection and the π^0 reconstruction are studied with the control sample of $J/\psi \to \pi^+\pi^-\pi^0$ [33]. The systematic uncertainty in the photon selection is assigned as 1.0% per photon, and the systematic uncertainty in the π^0 reconstruction, including the photon finding algorithm, the π^0 mass window and the 1C kinematic fit, is assigned as 2.0% per π^0.

The systematic uncertainty related to the $M_{\rm sig}$ fit has two sources. First, an alternative signal shape is obtained by varying the parameters of the smeared Gaussian function by $\pm1\sigma$. Second, an alternative background shape is obtained by varying the $q\bar{q}$ component in the inclusive MC sample by its uncertainty due to the limited MC statistics. For the upper limit determination of $D_s^+ \to K^+K^+\pi^-\pi^0$, the signal and background shape affect the likelihood function directly. Changing the signal (background) shape shifts the signal yield from the fit by 0.1 (0.2), and we take the larger value as the additive systematic uncertainty.

Varying the D_s^* branching fractions [12] by $\pm1\sigma$ changes the efficiency by 0.3%; this is taken as the associated uncertainty.

The systematic uncertainty related to the MC model is estimated using alternative signal MC samples. For $D_s^+ \to K^+K^+\pi^-$, the branching fraction of the $D_s^+ \to K^+K^{*0}$ subchannel is varied by its uncertainty. For $D_s^+ \to K^+K^+\pi^-\pi^0$, the average signal efficiency of $D_s^+ \to K^{*0}K^+\pi^0$, $K^{*+}K^+\pi^-$, $K^+K^+\rho^-$, and $D_s^+ \to K^+K^+\pi^-\pi^0$ (phase space) is used in place of the phase space efficiency. The maximum changes of the signal efficiencies, 0.7% and 5.3%, are assigned as the systematic uncertainties for $D_s^+ \to K^+K^+\pi^-$ and $D_s^+ \to K^+K^+\pi^-\pi^0$, respectively.

VII. RESULTS

Inserting the numbers of $N_{\rm DT}$, $N_{\rm ST}$, and $\epsilon_{\rm sig}$ of $D_s^+ \to K^+K^+\pi^-$ in Eq. (1), we determine its decay branching fraction to be

$$\mathcal{B}_{D_s^+\to K^+K^+\pi^-} = (1.24^{+0.28}_{-0.26}(\mathrm{stat}) \pm 0.06(\mathrm{syst})) \times 10^{-4}.$$

The upper limit on the branching fraction of $D_s^+ \to K^+K^+\pi^-\pi^0$ is set with the Bayesian approach [34], incorporating the systematic uncertainties. The raw likelihood distribution versus the branching fraction is smeared by a Gaussian function with a mean of zero and a width equal to the systematic uncertainty. The red solid curve in Fig. 4 shows the resulting likelihood distribution. The upper limit on the branching fraction at 90% confidence level is set as

$$\mathcal{B}_{D_s^+\to K^+K^+\pi^-\pi^0} < 1.7 \times 10^{-4}.$$

VIII. SUMMARY

Using 7.33 fb^{-1} of e^+e^- collision data collected at $E_{\rm c.m.}$ between 4.128 and 4.226 GeV with the BESIII detector, we investigate the DCS decays $D_s^+ \to K^+K^+\pi^-$ and $D_s^+ \to K^+K^+\pi^-\pi^0$. The absolute branching fraction of $D_s^+ \to K^+K^+\pi^-$ is determined to be $(1.24^{+0.28}_{-0.26}(\mathrm{stat}) \pm 0.06(\mathrm{syst})) \times 10^{-4}$, which is in good agreement with the world average value of $(1.274 \pm 0.031) \times 10^{-4}$ [12], based on the *relative* measurements from LHCb, *BABAR*, Belle, and FOCUS [13–16]. No significant signal of $D_s^+ \to K^+K^+\pi^-\pi^0$ is observed. The upper limit on the branching fraction of $D_s^+ \to K^+K^+\pi^-\pi^0$ is 1.7×10^{-4} at 90% confidence level. Table IV summarizes

TABLE IV. The branching fraction and upper limit obtained in this work, the world average branching fractions of the corresponding CF decays, the DCS/CF branching fraction ratios and these ratios in units of $\tan^4\theta_C$. The DCS/CF branching fraction ratios are consistent with the native expectation of $(0.5–2.0) \times \tan^4\theta_C$.

DCS decay	$\mathcal{B}_{\rm DCS}^{\rm this\ work}$ $(\times10^{-4})$	CF decay	$\mathcal{B}_{\rm CF}^{\rm PDG}$ $(\times10^{-2})$	$\mathcal{B}_{\rm DCS}^{\rm this\ work}/\mathcal{B}_{\rm CF}^{\rm PDG}$ $(\times10^{-3})$	$\times\tan^4\theta_{\rm C}$
$D_s^+ \to K^+K^+\pi^-$	$1.24^{+0.28}_{-0.26} \pm 0.06$	$D_s^+ \to K^+K^-\pi^+$	5.37 ± 0.10	$2.31^{+0.52}_{-0.48}$	$0.80^{+0.18}_{-0.16}$
$D_s^+ \to K^+K^+\pi^-\pi^0$	< 1.7	$D_s^+ \to K^+K^-\pi^+\pi^0$	5.50 ± 0.24	< 3.09	< 1.07

the results obtained in this work and the world average branching fractions of the corresponding CF decays. The DCS/CF branching fraction ratios and the corresponding factors relative to $\tan^4\theta_C$ are also listed. No significant deviation from native expectation of $(0.5-2.0)\times\tan^4\theta_C$ is found.

ACKNOWLEDGMENTS

The BESIII collaboration thanks the staff of BEPCII and the IHEP computing center for their strong support. This work is supported in part by National Key R&D Program of China under Contracts No. 2020YFA0406400, No. 2020YFA0406300; National Natural Science Foundation of China (NSFC) under Contracts No. 11635010, No. 11735014, No. 11835012, No. 11935015, No. 11935016, No. 11935018, No. 11961141012, No. 12025502, No. 12035009, No. 12035013, No. 12061131003, No. 12192260, No. 12192261, No. 12192262, No. 12192263, No. 12192264, No. 12192265, No. 12221005, No. 12225509, and No. 12235017; the Chinese Academy of Sciences (CAS) Large-Scale Scientific Facility Program; the CAS Center for Excellence in Particle Physics (CCEPP); Joint Large-Scale Scientific Facility Funds of the NSFC and CAS under Contracts No. U1932102, No. U1832207; CAS Key Research Program of Frontier Sciences under Contracts No. QYZDJ-SSW-SLH003, No. QYZDJ-SSW-SLH040; 100 Talents Program of CAS; The Institute of Nuclear and Particle Physics (INPAC) and Shanghai Key Laboratory for Particle Physics and Cosmology; European Union's Horizon 2020 research and innovation programme under Marie Sklodowska-Curie grant agreement under Contract No. 894790; German Research Foundation DFG under Contract No. 455635585, Collaborative Research Center CRC 1044, FOR5327, GRK 2149; Istituto Nazionale di Fisica Nucleare, Italy; Ministry of Development of Turkey under Contract No. DPT2006K-120470; National Research Foundation of Korea under Contract No. NRF-2022R1A2C1092335; National Science and Technology fund of Mongolia; National Science Research and Innovation Fund (NSRF) via the Program Management Unit for Human Resources & Institutional Development, Research and Innovation of Thailand under Contract No. B16F640076; Polish National Science Centre under Contract No. 2019/35/O/ST2/02907; The Swedish Research Council; U.S. Department of Energy under Contract No. DE-FG02-05ER41374.

[1] H. Y. Cheng and C. W. Chiang, Phys. Rev. D **81**, 074021 (2010).
[2] H. J. Lipkin, Nucl. Phys. B, Proc. Suppl. **115**, 117 (2003).
[3] M. Ablikim *et al.* (BESIII Collaboration), Phys. Rev. Lett. **125**, 141802 (2020).
[4] M. Ablikim *et al.* (BESIII Collaboration), Phys. Rev. D **104**, 072005 (2021).
[5] Z. z. Xing, Mod. Phys. Lett. **34A**, 1950238 (2019).
[6] H. J. Lipkin, Phys. Rev. Lett. **46**, 1307 (1981).
[7] Q. Qin, H. n. Li, C. D. Lü, and F. S. Yu, Phys. Rev. D **89**, 054006 (1981).
[8] H. Y. Cheng, C. W. Chiang, and A. L. Kuo, Phys. Rev. D **93**, 114010 (2016).
[9] W. Kwong and S. P. Rosen, Phys. Lett. B **298**, 413 (1993).
[10] Y. Grossman and D. J. Robinson, J. High Energy Phys. 04 (2013) 067.
[11] H. n. Li, C. D. Lü, and F. S. Yu, Phys. Rev. D **86**, 036012 (2012).
[12] P. A. Zyla *et al.* (Particle Data Group), Prog. Theor. Exp. Phys. **2022**, 083C01 (2022).
[13] R. Aaij *et al.* (LHCb Collaboration), J. High Energy Phys. 03 (2019) 176.
[14] P. del Amo Sanchez *et al.* (*BABAR* Collaboration), Phys. Rev. D **83**, 052001 (2011).
[15] B. R. Ko *et al.* (Belle Collaboration), Phys. Rev. Lett. **102**, 221802 (2009).
[16] J. M. Link *et al.* (FOCUS Collaboration), Phys. Lett. B **624**, 166 (2005).
[17] B. C. Ke, J. Koponen, H. B. Li, and Y. Zheng, Annu. Rev. Nucl. Part. Sci. **73**, 285 (2023).
[18] M. Ablikim *et al.* (BESIII Collaboration), Nucl. Instrum. Methods Phys. Res., Sect. A **614**, 345 (2010).
[19] C. H. Yu *et al.*, *Proceedings of IPAC2016* (Busan, Korea, 2016).
[20] P. Cao *et al.*, Nucl. Instrum. Methods Phys. Res., Sect. A **953**, 163053 (2020).
[21] M. Ablikim *et al.* (BESIII Collaboration), Chin. Phys. C **40**, 063001 (2016).
[22] M. Ablikim *et al.* (BESIII Collaboration), Chin. Phys. C **45**, 103001 (2020).
[23] S. Agostinelli *et al.* (GEANT4 Collaboration), Nucl. Instrum. Methods Phys. Res., Sect. A **506**, 250 (2003).
[24] S. Jadach, B. F. L. Ward, and Z. Was, Comput. Phys. Commun. **130**, 260 (2000); Phys. Rev. D **63**, 113009 (2001).
[25] D. J. Lange, Nucl. Instrum. Methods Phys. Res., Sect. A **462**, 152 (2001); R. G. Ping, Chin. Phys. C **32**, 599 (2008).
[26] J. C. Chen, G. S. Huang, X. R. Qi, D. H. Zhang, and Y. S. Zhu, Phys. Rev. D **62**, 034003 (2000).
[27] E. Richter-Was, Phys. Lett. B **303**, 163 (1993).

[28] R. M. Baltrusaitis *et al.* (MARKIII Collaboration), Phys. Rev. Lett. **56**, 2140 (1986); J. Adler *et al.* (MARKIII Collaboration), Phys. Rev. Lett. **60**, 89 (1988).
[29] M. Ablikim *et al.* (BESIII Collaboration), Phys. Rev. Lett. **122**, 071802 (2019).
[30] M. Ablikim *et al.* (BESIII Collaboration), Phys. Rev. Lett. **122**, 121801 (2019).
[31] M. Ablikim *et al.* (BESIII Collaboration), Phys. Rev. D **99**, 072002 (2019).
[32] M. Ablikim *et al.* (BESIII Collaboration), Phys. Rev. D **99**, 091101 (2019).
[33] M. Ablikim *et al.* (BESIII Collaboration), Phys. Rev. D **83**, 112005 (2011).
[34] K. Stenson, arXiv:physics/0605236.